Tight-binding parameters and exchange integrals of $Ba_2Cu_3O_4Cl_2$

H. Rosner and R. Hayn
Max Planck Arbeitsgruppe ''Elektronensysteme,'' Technische Universität Dresden, D-01062 Dresden, Federal Republic of Germany

J. Schulenburg
Institut für Theoretische Physik, Universität Magdeburg, D-39016 Magdeburg, Federal Republic of Germany

(Received 6 May 1997; revised manuscript received 23 December 1997)

Band-structure calculations of $Ba_2Cu_3O_4Cl_2$ within the local-density approximation (LDA) are presented. The investigated compound is similar to the antiferromagnetic parent compounds of the cuprate superconductors but contains additional Cu_B atoms in the Cu-O planes. Within the LDA, metallic behavior is found with two bands crossing the Fermi surface. These bands are built mainly from Cu $3d_{x^2-y^2}$ and O $2p_{x,y}$ orbitals, and a corresponding tight-binding (TB) model for these bands has been parameterized. All orbitals can be subdivided in two sets corresponding to the *A* and *B* subsystems, respectively, the coupling between which is found to be small. To describe the experimentally observed antiferromagnetic insulating state, we propose an extended Hubbard model using the parameters derived from the TB fit and local correlation terms characteristic for cuprates. Using this parameter set we calculate the exchange integrals for the Cu_3O_4 plane, the results being in quite reasonable agreement with the experimental values for the isostructural compound $Sr_2Cu_3O_4Cl_2$. [S0163-1829(98)009−22-9]

I. INTRODUCTION

Several new cuprate materials have been studied in the last years which contain modifications to the standard CuO_2 plane. This class includes not only the now-famous ladder compounds $Sr_{n-1}Cu_{n+1}O_{2n}$,[1] but also $Ba_2Cu_3O_4Cl_2$ or the similar $Sr_2Cu_3O_4Cl_2$.[2–5] The latter two compounds are antiferromagnetic insulators which are characterized by a Cu_3O_4 plane with additional Cu_B atoms in the standard Cu_AO_2 plane (Figs. 1 and 6). This new class of cuprates is currently of great scientific interest since it may shed light on some of the open questions in high-T_c superconductivity. The layered cuprate $Ba_2Cu_3O_4Cl_2$ itself is also interesting due to its rich magnetic structure and the unconventional character of its lowest energy excitations. Experimentally, two Néel temperatures have been found $T_N^A \sim 330$ K and $T_N^B \sim 31$ K (Refs. 3 and 6) connected with the two sublattices of *A* and *B* copper. The magnetic susceptibility and the small ferromagnetic moment have been explained phenomenologically[7] together with a determination of the exchange integrals. Like in undoped $Sr_2CuO_2Cl_2$,[8] the lowest electron removal states in $Ba_2Cu_3O_4Cl_2$ can be interpreted in terms of Zhang-Rice singlets[9] with a new branch of singlet excitations connected with the *B* sublattice.[10]

One might expect that the additional Cu_B would give rise to considerable differences in the electronic structure in comparison with the usual CuO_2 plane. In particular, the amount of coupling between both subsystems would appear to be crucial. This question will be addressed here by a microscopic investigation starting from a band-structure calculation. However, as for most undoped cuprates, the local-density approximation (LDA) leads to metallic behavior, and one has to treat the electron correlation in a more explicit way. In this paper, we use band-structure calculations to determine tight-binding (TB) parameters and then add the local Coulomb correlation terms. We present here a considerable improvement of the preliminary TB fit[11] where only the upper two bands had been fitted. Furthermore we also determine the weight of each of the relevant orbitals in the band structure (Sec. II) to obtain the TB parameters (Sec. III). In contrast to Ref. 11 we now distinguish between different oxygen orbitals. With reasonable assumptions about the local Coulomb correlation terms we estimate the exchange integrals in Sec. IV.

II. BAND-STRUCTURE CALCULATION

The tetragonal unit cell of $Ba_2Cu_3O_4Cl_2$ is shown in Fig. 1. We performed LDA calculations for this substance using the linear combination of atomiclike orbitals (LCAO). Due to the relatively open structure, eight empty spheres per unit cell (between Cu_A and Cl) have been introduced. The calculation was scalar relativistic and we have chosen a minimal basis set consisting of Cu($4s$,$4p$,$3d$), O($2s$,$2p$), Ba($6s$, $6p$,$5d$), and Cl($3s$,$3p$) orbitals, the lower lying states were treated as core states. To optimize the local basis, a contraction potential has been used at each site.[12] The exchange and correlation part was treated in the atomic-sphere approximation, while the Coulomb part of the potential was constructed as a sum of overlapping extended site potentials. Hence, this part of nonspherical effects determined by the crystal symmetry is taken into account self-consistently. On the other hand, the intra-atomic asphericity is suppressed by azimuthal averaging over the site-charge density during the iterations. The intra-atomic asphericity is only taken into account in the final step of calculating the weights of several orbitals in the band structure. These weights are necessary for an improvement of the preliminary TB fit.[11]

In our calculation the Bloch wave function $|\mathbf{k}\nu\rangle$ is composed of overlapping atomiclike orbitals $|Lij\rangle$ centered at

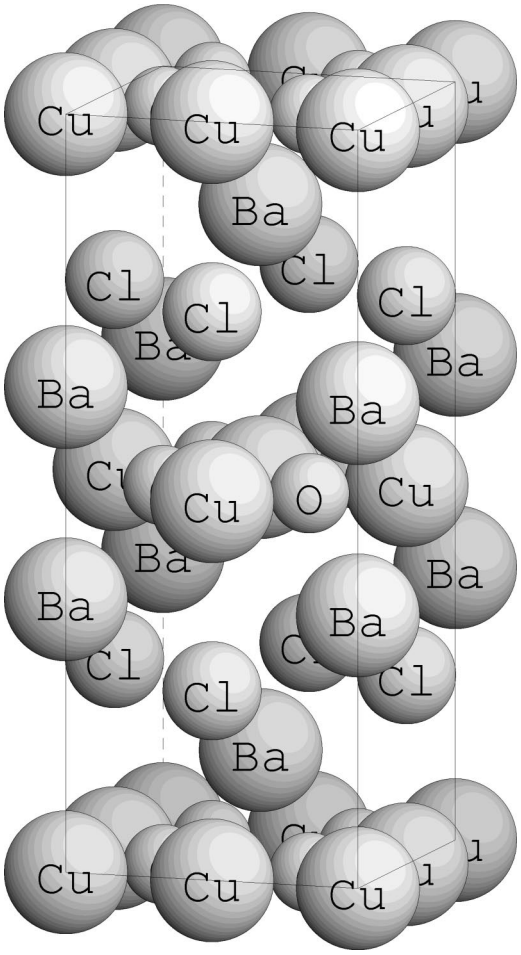

FIG. 1. The body-centered-tetragonal unit cell of $Ba_2Cu_3O_4Cl_2$ with lattice constants $a=5.51$ Å and $c=13.82$ Å.

the atomic site j in the elementary cell i with coordinates $\mathbf{R}_i+\mathbf{S}_j$,

$$|\mathbf{k}\nu\rangle=\sum_{Lij} C_{Lij}^{\mathbf{k}\nu}e^{i\mathbf{k}(\mathbf{R}_i+\mathbf{S}_j)}|Lij\rangle \tag{1}$$

with the normalization condition $\langle\mathbf{k}\nu|\mathbf{k}\nu\rangle=1$. Here, $L=\{nlm\}$ where n, l, and m denote the main quantum number, the angular momentum, and the magnetic quantum numbers, respectively. Note that for each l only one main quantum number n is considered. With the usual definition for the density of states

$$\rho(\omega)=\frac{1}{N_{\mathbf{k}}}\sum_{\mathbf{k}\nu}\int d^3r\langle\mathbf{k}\nu|\mathbf{r}\rangle\langle\mathbf{r}|\mathbf{k}\nu\rangle\delta(\omega-E_{\mathbf{k}\nu}), \tag{2}$$

where $N_{\mathbf{k}}$ is the number of elementary cells equivalent to the number of $\mathbf{k}$ values, one can write ρ as

$$\rho(\omega)=\frac{1}{N_{\mathbf{k}}}\sum_{\mathbf{k}\nu}\int d^3r\sum_{Lij}\sum_{L'i'j'} C_{Lij}^{\mathbf{k}\nu}C_{L'i'j'}^{\mathbf{k}\nu *}\langle Lij|\mathbf{r}\rangle \times\langle\mathbf{r}|L'i'j'\rangle e^{i\mathbf{k}(\mathbf{R}_i+\mathbf{S}_j-\mathbf{R}_{i'}-\mathbf{S}_{j'})}\delta(\omega-E_{\mathbf{k}\nu}) \tag{3}$$

or

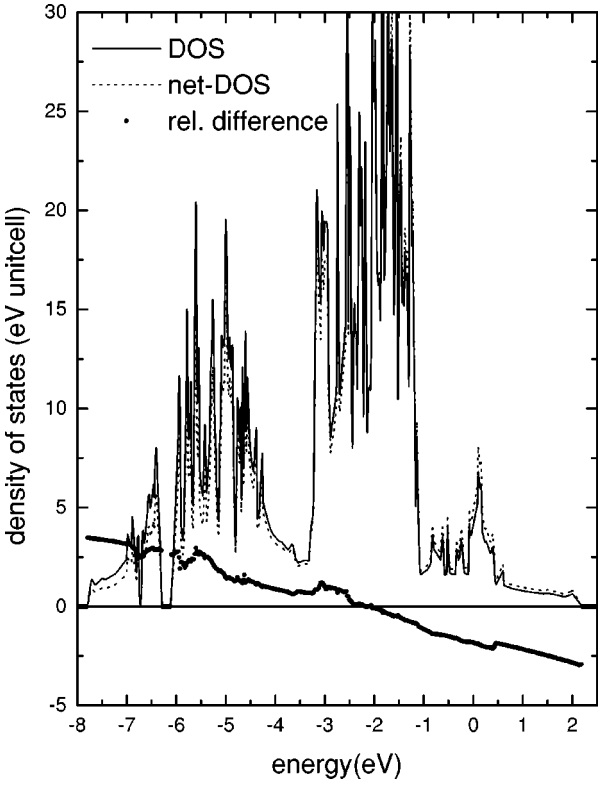

FIG. 2. LCAO-LDA DOS ρ (solid line) and net-DOS ρ_{net} (dashed line) of $Ba_2Cu_3O_4Cl_2$, the Fermi level is at zero energy. The scaled relative difference $[10(\rho-\rho_{\text{net}})/\rho]$ is plotted with large black dots.

$$\rho(\omega)=\frac{1}{N_{\mathbf{k}}}\sum_{\mathbf{k}\nu}\sum_{Lij}\sum_{L'i'j'} C_{Lij}^{\mathbf{k}\nu}C_{L'i'j'}^{*\mathbf{k}\nu}S_{Lij,L'i'j'} \times e^{i\mathbf{k}(\mathbf{R}_i+\mathbf{S}_j-\mathbf{R}_{i'}-\mathbf{S}_{j'})}\delta(\omega-E_{\mathbf{k}\nu}), \tag{4}$$

where $S_{Lij,L'i'j'}$ is the overlap matrix. Now one can decompose ρ into an on-site part ($i=i'$ and $j=j'$) and an overlap part ($i\neq i'$ or $j\neq j'$). For the on-site part one finds $S_{Lij,L'ij}=\delta_{LL'}$ due to the orthogonality of atomiclike orbitals at the same site. So we can define a net density of states (net-DOS)

$$\rho_{\text{net}}(\omega)=\frac{1}{N_{\mathbf{k}}}\sum_{\mathbf{k}\nu}\sum_{Lij}|C_{Lij}^{\mathbf{k}\nu}|^2\delta(\omega-E_{\mathbf{k}\nu}). \tag{5}$$

The difference between DOS and net-DOS consists in the overlap density but this difference is not very large as can be seen from Fig. 2. In the middle of the spectrum both quantities are nearly identical, whereas in the lower part the overlap density is positive and in the upper half the overlap density is negative such that the net-DOS becomes larger than the DOS. The relative difference $(\rho-\rho_{\text{net}})/\rho$ depends on the energy in an approximately linear way.

The band structure corresponding to the DOS of Fig. 2 is shown in Fig. 3(a). Its main result are two bands crossing the Fermi surface (FS). These two bands, in common with most of the other bands, show nearly no dispersion in the z direction which justifies the restriction to the Cu_3O_4 plane in the following discussion. The two bands give rise to a peak in

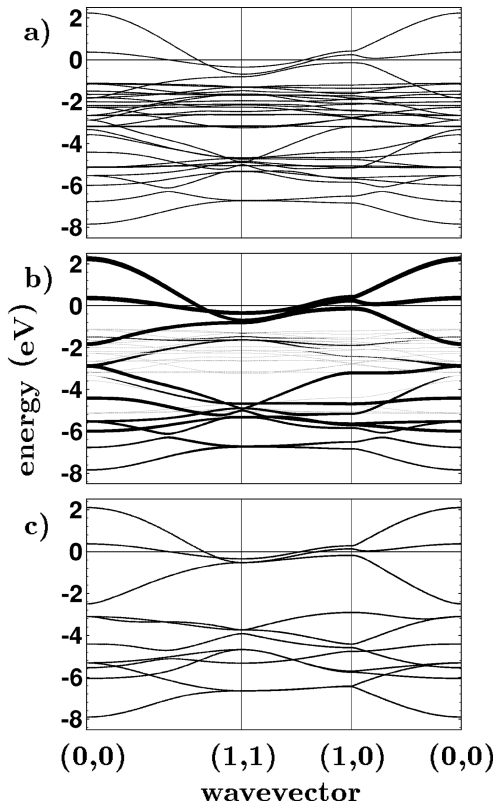

FIG. 3. (a) LCAO-LDA band structure of the Cu_3O_4 plane of $Ba_2Cu_3O_4Cl_2$, the Fermi level is at zero energy. (b) The same as in (a), but the weight of the lines is scaled with the sum of all 11 orbital projections that are used in the TB model. (c) The band structure of the TB model. The parameter set used is shown in Table I. The wave vector is measured in units of $(\pi/a,\pi/a)$.

the DOS (Fig. 2) at the Fermi level. To analyze the orbital character of the two relevant bands, we write the net-DOS (5) as

$$\rho_{\rm net}(\omega)=\frac{1}{N_{\mathbf{k}}}\sum_{\mathbf{k}\nu}\sum_{Lj} W_{Lj}^{\mathbf{k}\nu}\delta(\omega-E_{\mathbf{k}\nu}), \tag{6}$$

where we define the weight of the orbital $|Lj\rangle$ in the state $|\mathbf{k}\nu\rangle$ in the form:

$$W_{Lj}^{\mathbf{k}\nu}=\sum_i |C_{Lij}^{\mathbf{k}\nu}|^2. \tag{7}$$

The sum of all weights is approximately unity, $\Sigma_{Lj}W_{Lj}^{\mathbf{k}\nu}\approx 1$, with deviations due to the neglect of the overlap density which are linear in energy (see Fig. 2 and the discussion above).

In Figs. 4(a) and 4(b) we show the weights of the Cu_A $3d_{x^2-y^2}$ and Cu_B $3d_{x^2-y^2}$ orbitals, respectively. We can observe that the broadband is built up of predominantly the Cu_A $3d_{x^2-y^2}$ orbital which hybridizes with one part of the planar oxygen $2p_{x,y}$ orbitals resulting in $dp\sigma$ bonds. The corresponding oxygen orbitals, directed to the Cu_A atoms, are denoted here as p_σ orbitals. Their weight is shown in Fig. 5(a). The p_σ orbitals are to be distinguished from the oxygen p_π orbitals [Fig. 5(b)] which are perpendicular to them[13] (see Fig. 6). These oxygen p_π orbitals hybridize with Cu_B $3d_{x^2-y^2}$, building the narrow band at the FS [see Fig. 4(b)].

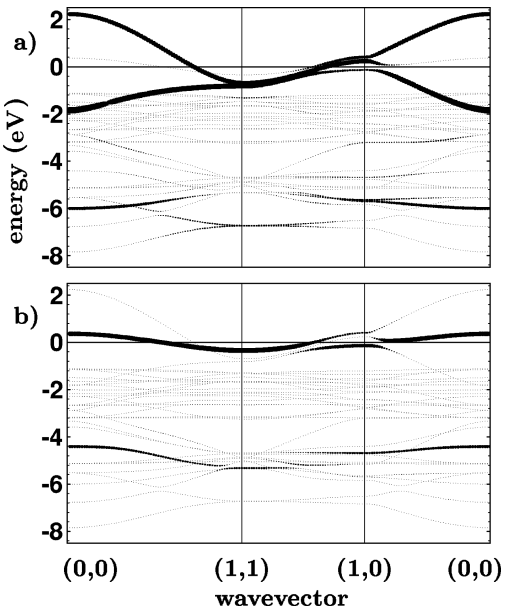

FIG. 4. Weight of (a) Cu_A $3d_{x^2-y^2}$ and (b) Cu_B $3d_{x^2-y^2}$ orbitals in the LCAO-LDA band structure of $Ba_2Cu_3O_4Cl_2$. The wave vector is measured in units of $(\pi/a,\pi/a)$.

There is generally very small weight of the p_σ orbitals in this narrow band, indicating that there is only small coupling between the A and B subsystems. The only exception to this occurs around the wave vector $(\pi/a,0)$. A further analysis shows that the band complex between -1 and -3 eV is predominantly built up of out-of-plane oxygen p_z together with the corresponding Cu $3d_{xz,yz}$ orbitals (not shown), as well as a large contribution of Cl derived states.[11] The in-plane oxygen orbitals contribute mainly to the lower band complex between -4 and -8 eV [see Figs. 5(a) and 5(b)].

Thus it is evident that the two bands crossing the FS which we want to analyze have nearly pure $3d_{x^2-y^2}$ and $2p_{x,y}$ character.[14] Therefore, we have to consider all together

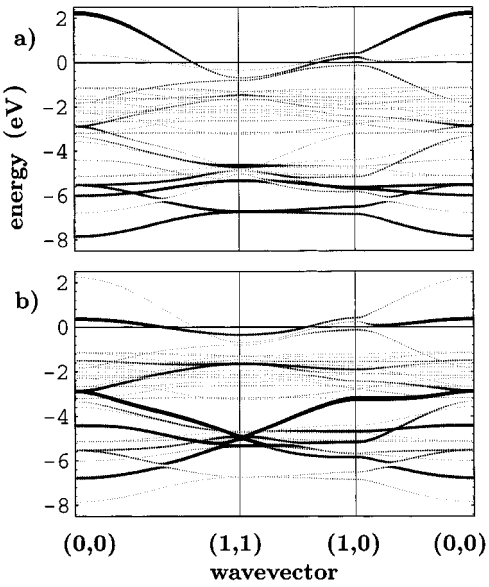

FIG. 5. Weight of (a) O $2p_\sigma$ and (b) O $2p_\pi$ orbitals in the LCAO-LDA band structure of $Ba_2Cu_3O_4Cl_2$. The wave vector is measured in units of $(\pi/a,\pi/a)$.

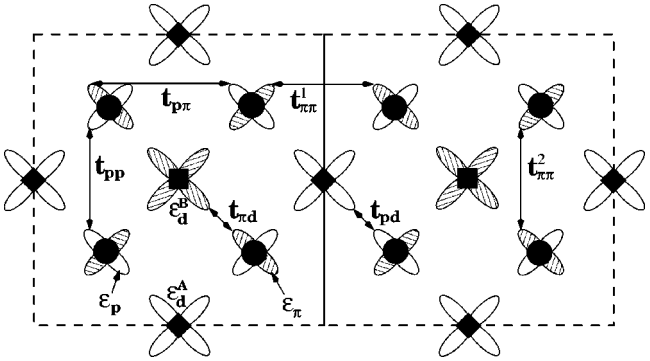

FIG. 6. Two elementary cells of the Cu_3O_4 plane in $Ba_2Cu_3O_4Cl_2$ or $Sr_2Cu_3O_4Cl_2$ and the Cu $3d_{x^2-y^2}$ and O $2p_{x,y}$ orbitals comprising the TB model. Also shown are the corresponding transfer integrals t_{pd}, $t_{\pi d}$, t_{pp}, $t^1_{\pi\pi}$, $t^2_{\pi\pi}$, and $t_{p\pi}$. The Cu_A orbitals with on-site energy ε^A_d are marked by black diamonds, the Cu_B orbitals with on-site energy ε^B_d by black squares and the two different kinds of O orbitals with on-site energies ε_p and ε_π, respectively, by black circles. The orbitals of the *B* subsystem are shaded to distinguish them from the orbitals of the *A* subsystem (white).

11 orbitals in the elementary cell of Cu_3O_4, namely two Cu_A $3d_{x^2-y^2}$, one Cu_B $3d_{x^2-y^2}$, four oxygen p_σ and four oxygen p_π orbitals. In Fig. 3(b) we pick out the corresponding bands from the LDA band structure for which the sum of all 11 orbital weights [Eq. (7)] is large. It is seen that the sum of all orbital projections in Fig. 3(b) decreases with increasing binding energy. That can be explained by the reasons mentioned above. One can also observe that the lower eight bands in Fig. 3(b) are not as pure as the upper three. For the upper bands only a very small weight of additional orbitals, in particular Cu 4*s* contributions, has been detected. These contributions are neglected in the following.

III. TIGHT-BINDING PARAMETERS

It is our main goal to find a TB description of the relevant bands crossing the FS. This task is difficult due to the large number of bands between -1 and -8 eV of Fig. 3(a). There is no isolated band complex which makes a TB analysis easy. However we have pointed out already that the relevant bands are a nearly pure combination of Cu $3d_{x^2-y^2}$ and O $2p_{x,y}$ orbitals. Thus we will only concentrate on these orbitals, thereby accepting some deviations in the lower band complex between -3 and -8 eV. The relevant orbitals are depicted in Fig. 6. The tight-binding Hamiltonian H_{TB} can be written as a sum of three parts:

$$H_{\mathrm{TB}}=H_A+H_B+H_{AB}. \tag{8}$$

We distinguish two classes of orbitals corresponding to the two different subsystems. One consists of Cu_A $3d_{x^2-y^2}$ orbitals at the sites **R** with on-site energies ε^A_d and oxygen $2p_\sigma$ orbitals at the sites **r** with ε_p:

$$\begin{aligned} H_A=&\varepsilon^A_d\sum_{\mathbf{R}s} d^\dagger_{\mathbf{R}s}d_{\mathbf{R}s}+\varepsilon_p\sum_{\mathbf{r}s} p^\dagger_{\mathbf{r}s}p_{\mathbf{r}s}\\ &+t_{pd}\sum_{\substack{\mathbf{Rr}\\ s}} (\alpha_{\mathbf{Rr}}d^\dagger_{\mathbf{R}s}p_{\mathbf{r}s}+\mathrm{H.c.})\\ &+t_{pp}\sum_{\substack{\mathbf{rr'}\\ s}} (\alpha_{\mathbf{rr'}}p^\dagger_{\mathbf{r}s}p_{\mathbf{r'}s}+\mathrm{H.c.}), \end{aligned} \tag{9}$$

where $d^\dagger_{\mathbf{R}s}$ and $p^\dagger_{\mathbf{r}s}$ are the usual creation operators for Cu $3d_{x^2-y^2}$ and O $2p_\sigma$ orbitals, respectively, and $\alpha_{\mathbf{R}\mathbf{r}}$ is a phase factor corresponding to Fig. 6 which connects only neighboring sites. The other class incorporates Cu_B $3d_{x^2-y^2}$ orbitals at the sites **G** with on-site energies ε^B_d and oxygen p_π orbitals at the sites **r** with ε_π. One gets the Hamiltonian H_B by replacing **R** with **G**, and the on-site and transfer energies with the corresponding energies of the Cu_B subsystem, respectively. The creation operators $p^\dagger_{\mathbf{r}s}$ should then be replaced with the operators $\pi^\dagger_{\mathbf{r}s}$ thus creating an O $2p_\pi$ orbital. The coupling between both classes of orbitals, which correspond to the Cu_A and Cu_B subsystems, respectively, is provided by the parameter $t_{p\pi}$:

$$H_{AB}=t_{p\pi}\sum_{\substack{\mathbf{rr'}\\ s}} (\alpha_{\mathbf{rr'}}p^\dagger_{\mathbf{r}s}\pi_{\mathbf{r'}s}+\mathrm{H.c.}). \tag{10}$$

All together, we have to determine ten parameters, four on-site energies (ε^A_d, ε^B_d, ε_p, ε_π), the nearest-neighbor transfer integrals (t_{pd}, $t_{\pi d}$), and several kinds of oxygen transfers (t_{pp}, $t^1_{\pi\pi}$, $t^2_{\pi\pi}$, $t_{p\pi}$).

In our analysis we found that the Cu_A-Cu_B transfer t_{dd} can be neglected since its estimation yields a value smaller than 0.08 eV.[15] Each p_σ orbital is located between two Cu_A sites and we neglect the influence of different local environments on the t_{pp} transfer integral. In the case of the $t_{\pi\pi}$ transfer we distinguish the two possible local arrangements, but the numerical difference between $t^1_{\pi\pi}$ and $t^2_{\pi\pi}$ is small (see Table I). The necessity to distinguish between oxygen $2p_\sigma$ and $2p_\pi$ orbitals was pointed out by Mattheiss and Hamann[13] for the case of the standard CuO_2 plane.

TABLE I. Parameters of the TB fit and the proposed extended Hubbard model for the Cu_3O_4 plane in $Ba_2Cu_3O_4Cl_2$.

Parameter	ε^A_d	ε^B_d	ε_p	ε_π	t_{pd}	$t_{\pi d}$	t_{pp}	$t^1_{\pi\pi}$	$t^2_{\pi\pi}$	$t_{p\pi}$	U_d	U_p	U_{pd}	$U_{p\pi}$	K_{pd}	$K_{p\pi}$
TB fit (electron representation) (energy/eV)	−2.50	−2.12	−4.68	−3.73	1.43	1.19	0.81	0.41	0.50	0.25	-	-	-	-	-	-
Extended Hubbard model (hole representation) (energy eV)	2.50	2.12	6.68	5.73	−1.43	−1.19	−0.81	−0.41	−0.50	−0.25	10.5	4.0	1.2	3.2	−0.18	−0.4

Since there is a considerable admixture of other orbitals, especially Cu $3d_{xy}$ and Cu $3d_{3z^2-r^2}$, in some of the lower bands of Fig. 3(b), we cannot determine the ten TB parameters by a least-square fits of the 11 TB bands to the heavily shaded LDA bands of Fig. 3(b). Instead, at the high-symmetry points $\Gamma=(0,0)$ and $M=(\pi/a,\pi/a)$ we picked out those bands in Fig. 3(b) which have the most pure $3d_{x^2-y^2}$ and $2p_{x,y}$ character. Only those energies were compared with the TB band structure [Fig. 2(c)] derived by diagonalizing a 11×11 matrix. In this way it is possible to calculate the parameter set analytically because the TB matrix splits up into 3×3 and 4×4 matrices at the high-symmetry points $\Gamma=(0,0)$ and $M=(\pi/a,\pi/a)$. The calculated eigenvalues are given in the Appendix A. That procedure results in the parameters given in Table I. These values are similar to those which are known for the standard CuO_2 plane. The largest transfer integrals are $t_{pd}=1.43$ eV and $t_{\pi d}=1.19$ eV as expected. Nevertheless these values are somewhat smaller than in the previous TB fit[11] where all oxygen orbitals were treated as identical. The difference between t_{pp} and $t_{\pi\pi}$ is roughly a factor of 2 in coincidence with the situation in the standard CuO_2 plane,[13] a fact which was not taken into account in Ref. 11. We have found that only the smallest parameter, $t_{p\pi}=0.25$ eV, is responsible for the coupling between the subsystems of Cu_A and Cu_B. Thus despite the fact that the two oxygen p_σ and p_π orbitals are located in real space at the same atom, they are quite far away from each other in Hilbert space.

IV. EXCHANGE INTEGRALS

Thus far we have found that the TB parameters are rather similar to the standard CuO_2 case and that the coupling between the Cu_A and Cu_B subsystem is quite small. This justifies the usage of standard parameters for the Coulomb interaction part of the Hamiltonian. Of course it would be desirable to determine these values by a constrained density-functional calculation for $Ba_2Cu_3O_4Cl_2$, but we expect only small changes in the estimation of exchange integrals presented below.

The Coulomb interaction also changes the on-site copper and oxygen energies. Their difference, given in the first line of Table I, is too small to explain the charge-transfer gap of ~2 eV in $Ba_2Cu_3O_4Cl_2$.[16] Adding 2 eV to the on-site oxygen energies, the difference $\Delta=\varepsilon_p-\varepsilon_d^A$ (in hole representation which is chosen from now on) becomes similar to the standard value derived by Hybertsen *et al.*[17] for La_2CuO_4. Our proposal of on-site energies for the multiband Hubbard model $H=H_{\rm TB}+H_{\rm int}$ are given in the second line of Table I. We have used the values of Ref. 17 also for the parameters of the Coulomb interaction part

$$H_{\rm int}=\sum_i U_i n_{i\uparrow}n_{i\downarrow}+\frac{1}{2}\sum_{\substack{ij\\ss'}} U_{ij}n_{is}n_{js'}+\sum_{ij} K_{ij}\mathbf{S}_i\mathbf{S}_j, \tag{11}$$

where n_{is} is the occupation operator of the orbital i with the spin s and $\mathbf{S_i}$ the corresponding spin operator. From Ref. 17 we know the values for U_d, U_p, U_{pd} and K_{pd}. Since we now have two oxygen orbitals at one site we also have to take into account the corresponding Hund's rule coupling energy which is in the notation of Eq. (11) $K_{p\pi}$. That correlation energy is not given in Ref. 17 and we use here the simple rule $K_{p\pi}=-0.1U_p$.[18] The Coulomb repulsion between two oxygen holes in p_σ and p_π orbitals is assumed to be $U_{p\pi}=U_p+2K_{p\pi}$, which is a valid approximation given degenerate orbitals. In the second line of Table I we combine the TB parameters derived from the band structure of $Ba_2Cu_3O_4Cl_2$ (now in hole representation) with the standard Coulomb correlation terms. This parameter set then defines an 11-band extended Hubbard model for the Cu_3O_4 plane which is used for the following estimation.

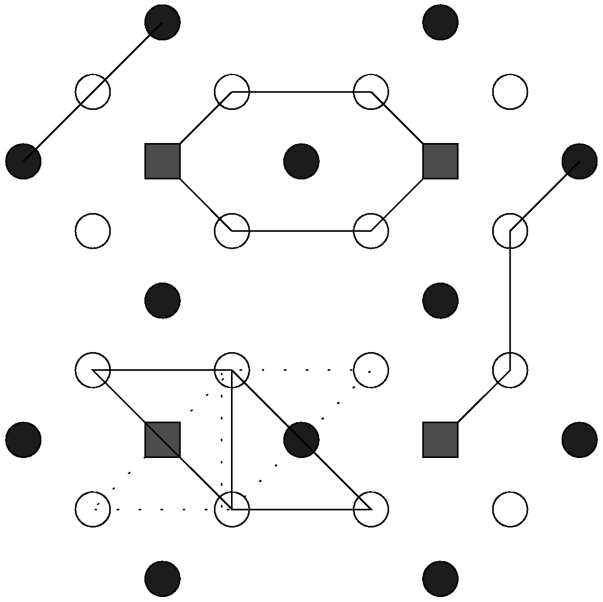

FIG. 7. Clusters used for the calculation of the exchange integrals J_{AA} (upper left), J_{BB} (upper middle), $J_{AB}^{(1)}$ (lower left) and $J_{AB}^{(3)}$ (lower right). The Cu_A sites are marked with filled circles, the Cu_B sites with squares and the oxygen sites with open circles.

The exchange integrals have been calculated using the usual Rayleigh-Schrödinger perturbation theory on small clusters (Fig. 7). All transfer integrals (and $K_{p\pi}$) have been considered as a perturbation around the local limit. We calculated all exchange integrals in the corresponding lowest order (see Appendix B). The exchange $J_{AA}\propto t_{pd}^4/\Delta^3$ between two Cu_A spins is given in fourth order for the simple Cu_A-O-Cu_A cluster. It turns out that the influence of intersite Coulomb and exchange terms U_{pd} and K_{pd} is rather large, decreasing J_{AA} from 246 to 99 meV (see Table II). In spite of

TABLE II. Different exchange integrals as explained in the text. Compared are estimations within the extended Hubbard model with experimental values (Ref. 7).

Exchange integral	Without $U_{pd}, K_{pd}, K_{p\pi}$ (meV)	All parameters (meV)	Experiment (meV)
J_{AA}	246	99	130 ± 40
J_{BB}	17	12	10 ± 1
$J_{AB,af}^{(1)}$	6.9	4.6	
$J_{AB,f}^{(1)}$		-20	
$J_{AB}^{(1)}$		-15	-12 ± 9
$J_{AB,af}^{(3)}$	1.4	0.8	

our rather approximate procedure, the latter value agrees quite reasonably with the phenomenological value (130 ± 40) meV (Ref. 7) for $Sr_2Cu_3O_4Cl_2$. J_{AA} is thus also quite close to the standard value of the CuO_2 plane [~ 140 meV (Ref. 17)].

The exchange J_{BB} is given only in sixth order for a larger cluster of two Cu_B, one Cu_A and four oxygen orbitals. Correspondingly, it is roughly one order of magnitude smaller, $J_{BB}\sim 12$ meV (Table II). For J_{AB} we need to distinguish between antiferromagnetic and ferromagnetic contributions. There are two antiferromagnetic couplings between nearest-neighbor copper atoms $J^{(1)}_{AB,af}$ and third-nearest-neighbor copper atoms $J^{(3)}_{AB,af}$, both being comparably small at 4.6 and 0.8 meV, respectively. The ferromagnetic contribution $J_{AB,f}=-20$ meV between nearest-neighbor copper spins arises in fifth order and is provided by Hund's rule coupling of two virtual oxygen holes sitting at the same oxygen. Since $K_{p\pi}$ is known with less accuracy than the other interaction parameters, this value has to be taken with care.

V. SUMMARY

Summarizing, we have presented an LCAO-LDA band-structure calculation for $Ba_2Cu_3O_4Cl_2$. Deriving TB parameters from it, we found only a weak coupling between the two sets of orbitals connected with the subsystems of copper A (Cu_A $3d_{x^2-y^2}$ and O $2p_\sigma$) and copper B (Cu_B $3d_{x^2-y^2}$ and O $2p_\pi$). Furthermore, we derived exchange integrals J_{AA}, J_{BB}, and J_{AB} in reasonable agreement[19] with phenomenologically derived values from magnetic-susceptibility data if we add to the TB parameters the standard local Coulomb correlation energies. One should note, however, that we used a rather approximate perturbative procedure to estimate the exchange integrals. We expect that the Rayleigh-Schrödinger perturbation theory provides us with the right order of magnitude, but it may fail in the correct numbers. In that sense the agreement of the theoretical exchange integrals with the experimental ones should not be overinterpreted. On the other hand, the TB parameters were obtained by fitting to a first-principles band structure and they are accurate within the chosen orbital set.

ACKNOWLEDGMENTS

Discussions with S.-L. Drechsler, H. Eschrig, J. Richter, J. Fink, H. Schmelz, and A. Aharony are acknowledged. Special thanks to M. S. Golden for discussions and a critical reading of the manuscript. H.R. acknowledges the *Graduiertenkolleg 'Struktur und Korrelationseffekte in Festkörpern' der TU Dresden (DFG).*

APPENDIX A: EIGENVALUES

As written in Sec. III, at the high-symmetry points $\Gamma=(0,0)$ and $M=(\pi/a,\pi/a)$ the tight-binding matrix is block diagonal, so it is possible to calculate the eigenvalues analytically. In the following these eigenvalues are listed corresponding to the different parts of the tight-binding Hamiltonian.

Eigenvalues at $\mathbf{k}=(0,0)$:

Cu_A subsystem:

$$\varepsilon_d^A,$$

$$\varepsilon_p-4t_{pp}, \tag{A1}$$

$$\frac{1}{2}[\varepsilon_d^A+\varepsilon_p+4t_{pp}\pm\sqrt{(\Delta_A+4t_{pp})^2+32t_{pd}^2}].$$

Cu_B subsystem:

$$\varepsilon_\pi-2t^+_{\pi\pi}, \tag{A2}$$

$$\frac{1}{2}[\varepsilon_d^B+\varepsilon_\pi+2t^+_{\pi\pi}\pm\sqrt{(\Delta_B+2t^+_{\pi\pi})^2+16t^2_{\pi d}}],$$

coupling between the subsystems:

$$1/2(\varepsilon_p+\varepsilon_\pi\pm\sqrt{\Delta^2_{p\pi}+64t^2_{p\pi}}). \tag{A3}$$

The eigenvalues in Eq. (A3) are twofold degenerated.

Eigenvalues at $\mathbf{k}=(\pi,\pi)$:

Cu_A subsystem:

$$\frac{1}{2}[\varepsilon_d^A+\varepsilon_p\pm\sqrt{\Delta_A^2+16t_{pd}^2}]. \tag{A4}$$

Cu_B subsystem:

$$\varepsilon_\pi+2t^-_{\pi\pi}, \tag{A5}$$

$$\frac{1}{2}[\varepsilon_d^B+\varepsilon_\pi-2t^-_{\pi\pi}\pm\sqrt{(\Delta_B-2t^-_{\pi\pi})^2+16t^2_{\pi d}}],$$

coupling between the subsystems:

$$\varepsilon_p, \tag{A6}$$

$$\varepsilon_\pi,$$

where $\Delta_A=\varepsilon_p-\varepsilon_d^A$, $\Delta_B=\varepsilon_\pi-\varepsilon_d^B$, $\Delta_{p\pi}=\varepsilon_p-\varepsilon_\pi$, $t^\pm_{\pi\pi}=t^1_{\pi\pi}\pm t^2_{\pi\pi}$. The eigenvalues in Eqs. (A4) and (A6) are twofold degenerated.

APPENDIX B: EXCHANGE INTEGRALS

$$\Delta_A=\varepsilon_p-\varepsilon_d^A,\quad \Delta_B=\varepsilon_\pi-\varepsilon_d^B,$$

$$\Delta_{AB}=\varepsilon_p-\varepsilon_d^B,\quad \Delta_{BA}=\varepsilon_\pi-\varepsilon_d^A, \tag{B1}$$

$$t_{pdA}=t_{pd},\quad t_{pdB}=t_{\pi d}, \tag{B2}$$

$$J^{[4]}_{AA}=\frac{4t^2_{pdA}}{(\Delta_A+U_{pd})^2}\times\left\{K_{pd}+\frac{2t^2_{pdA}}{2\Delta_A+U_p}+\frac{t^2_{pdA}}{U_d}+\frac{K^2_{pd}}{\Delta_A+U_{pd}}\right\}, \tag{B3}$$

$$J_{BB}^{[6]}=\frac{8t_{pdB}^2(t_{\pi\pi}^1)^2}{\Delta_B^2}\times\left\{\frac{1}{(\Delta_B+U_{pd})^2}\left(K_{pd}+\frac{2t_{pdB}^2}{U_d}\right)+\frac{K_{pd}^2}{(\Delta_B+U_{pd})^3}+t_{pdB}^2\left(\frac{1}{2\Delta_B+U_p}+\frac{1}{2\Delta_B}\right)\times\left(\frac{1}{\Delta_B+U_{pd}}+\frac{2}{2\Delta_B}\right)^2\right\}, \tag{B4}$$

$$J_{AB}^{(3)[6]}=\sum_{A\leftrightarrow B}\frac{2t_{p\pi}^2t_{pdB}^2K_{pd}}{\Delta_B^2(\Delta_{AB}+U_{pd})^2}\left(1+\frac{K_{pd}}{\Delta_{AB}+U_{pd}}\right)+\sum_{A\leftrightarrow B}\frac{2t_{p\pi}^2t_{pdA}^2t_{pdB}^2}{\Delta_B^2(\Delta_{AB}+\Delta_A+U_p)}\left(\frac{1}{\Delta_A}+\frac{1}{\Delta_{AB}+U_{pd}}\right)^2+\sum_{A\leftrightarrow B}\frac{2t_{p\pi}^2t_{pdA}^2t_{pdB}^2}{\Delta_B^2(\Delta_{AB}+U_{pd})^2(\varepsilon_d^A-\varepsilon_d^B+U_d)}, \tag{B5}$$

$$J_{AB,af}^{(1)[6]}=\sum_{A\leftrightarrow B}\frac{4t_{p\pi}^2t_{pdB}^2K_{pd}}{\Delta_B^2(\Delta_{AB}+U_{pd})^2}\left(1+\frac{K_{pd}}{\Delta_{AB}+U_{pd}}\right)+\sum_{A\leftrightarrow B}\frac{4t_{p\pi}^2t_{pdA}^2t_{pdB}^2}{\Delta_B^2(\Delta_A+\Delta_{AB})}\left(\frac{1}{\Delta_A}+\frac{1}{\Delta_{AB}+U_{pd}}\right)^2+\sum_{A\leftrightarrow B}\frac{4t_{p\pi}^2t_{pdA}^2t_{pdB}^2}{\Delta_B^2(\Delta_{AB}+\Delta_A+U_p)}\left(\frac{1}{\Delta_A}+\frac{1}{\Delta_{AB}+U_{pd}}\right)^2+\sum_{A\leftrightarrow B}\frac{8t_{p\pi}^2t_{pdA}^2t_{pdB}^2}{\Delta_B^2(\Delta_{AB}+U_{pd})^2(\varepsilon_d^A-\varepsilon_d^B+U_d)}, \tag{B6}$$

$$J_{AB,f}^{(1)[5]}=\frac{4t_{pdA}^2t_{pdB}^2 2K_{p\pi}}{(\Delta_A+\Delta_B+U_{p\pi})^2}\left(\frac{1}{\Delta_A}+\frac{1}{\Delta_B}\right)^2. \tag{B7}$$

[1] E. Dagotto and T. M. Rice, Science **271**, 618 (1996).

[2] R. Kipka and Hk. Müller-Buschbaum, Z. Anorg. Allg. Chem. **419**, 58 (1976).

[3] S. Noro *et al.*, Mater. Sci. Eng. B **25**, 167 (1994).

[4] H. Ohta *et al.*, J. Phys. Soc. Jpn. **64**, 1759 (1995).

[5] K. Yamada, N. Suzuki, and J. Akimitsu, Physica (Amsterdam) **213&214B**, 191 (1995).

[6] T. Ito, H. Yamaguchi, and K. Oka, Phys. Rev. B **55**, R684 (1997).

[7] F. C. Chou *et al.*, Phys. Rev. Lett. **78**, 535 (1997).

[8] B. O. Wells *et al.*, Phys. Rev. Lett. **74**, 964 (1995).

[9] F. C. Zhang and T. M. Rice, Phys. Rev. B **37**, 3759 (1988).

[10] M. S. Golden *et al.*, Phys. Rev. Lett. **78**, 4107 (1997).

[11] H. Rosner and R. Hayn, Physica B **230-232**, 889 (1997).

[12] H. Eschrig, *Optimized LCAO Method*, 1st ed. (Springer-Verlag, Berlin, 1989).

[13] L. F. Mattheiss and D. R. Hamann, Phys. Rev. B **40**, 2217 (1989).

[14] The corresponding band complex with nearly pure $3d_{x^2-y^2}$ and $2p_{x,y}$ character includes also a third band just below the FS. It has Cu_A $3d_{x^2-y^2}$ and O p_σ character similar to the broadband crossing the FS. This can be understood since there are two Cu_A in the elementary cell of Cu_3O_4.

[15] The parameter t_{dd} can be roughly estimated by the weight of the Cu_A in the Cu_B band crossing the Fermi level at the $\Gamma=(0,0)$ point of the Brillouin zone. At this point the coupling via $t_{p\pi}$ is not possible due to symmetry.

[16] O. Knauff *et al.*, J. Low Temp. Phys. **105**, 353 (1996).

[17] M. S. Hybertson, E. B. Stechel, M. Schlüter, and D. R. Jennison, Phys. Rev. B **41**, 11 068 (1990).

[18] A. M. Olés, Phys. Rev. B **28**, 327 (1983).

[19] The anisotropic coupling $J\sim 20$ μeV which was found to be responsible for the small ferromagnetic moment in $Sr_2Cu_3O_4Cl_2$ cannot be estimated within the model proposed here. It requires a more refined treatment incorporating spin-orbit coupling and more orbitals at the Cu site.